



## Chapter 1

# Matching algorithms with physics: exact sequences of finite element spaces

*P.B. Bochev\**, *A.C. Robinson<sup>†‡</sup>*

## 1.1 Introduction

In finite element lore the term “unstable discretization” is often applied to situations when approximate solutions develop unphysical “wiggles”, or otherwise behave in a strange manner. A textbook example of such wiggles are Galerkin solutions of a scalar hyperbolic equation with discontinuous data. A more subtle example of instability is the “strange” behavior of mixed finite elements for the Stokes problem when velocity and pressure are approximated by a linear-constant pair.

In both cases failure of finite element methods to produce an adequate solution stems from discretization defects, i.e., a choice of finite element spaces that is inconsistent with the problem being solved. For instance, oscillations in the Galerkin method are invoked by symmetric discretization of an advection operator, while the linear-constant pair violates the inf-sup stability condition required for well-posedness of saddle-point optimization problems. The presence of these defects in the finite element method will almost surely lead to a disaster and in that sense they represent strong stability threats.

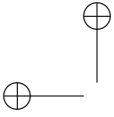
However, a finite element discretization may possess flaws which do not lead to an immediate and obvious failure. Examples include minute oscillations in SUPG methods, approximation of solenoidal fields by approximately divergence free vectors, and many other “small” infractions. Because the impact of these defects is, as

---

\*Sandia National Laboratories, Computational Math and Algorithms Department, P.O. Box 5800, MS 1110, Albuquerque, NM 87185-1110 ([pbboche@sandia.gov](mailto:pbboche@sandia.gov))

<sup>†</sup>Sandia National Laboratories, Computational Physics R&D Department, Box 5800, MS 0819, Albuquerque, NM 87185-0819 ([acrobins@sandia.gov](mailto:acrobins@sandia.gov)).

<sup>‡</sup>Sandia is a multiprogram laboratory operated by Sandia Corporation, a Lockheed Martin Company, for the United States Department of Energy under Contract DE-AC04-94AL85000.



a rule, confined within the local discretization error, they are routinely dismissed as being benign, at least compared with the defects mentioned above.

While this may be true for simple mathematical models, the presence of even small discretization defects often proves disastrous in large scale computations of complex multiphysics systems. Such systems are modelled by many interacting components that are coupled through interaction of forces, exchange of energy, momentum and may involve vastly different time scales. As a result, a “small” discretization defect in one of the components may be potentially amplified as it passes through the components of the system.

For such multiphysics problems managing complexity of fully coupled models is made more tractable by ensuring reliability and physical fidelity of each component before coupling it with the rest of the model. In this article we focus on our experiences in applying this strategy to numerical simulation of the Z-pinch. The Z-pinch is a technique for generating large material compressions and energies by generating a cylindrical implosion using focused magnetic field energy. Wire array implosions for example are used to generate extremely large X-ray power pulses [34]. A key component of the Z-pinch model, required to deliver usable simulations in three dimensions, is magnetic diffusion in heterogeneous conductors.

In what follows we consider, compare, and contrast two approaches to finite element modeling of magnetic diffusion which subscribe to fundamentally different philosophies. The first approach utilizes standard nodal finite element spaces and tries to achieve physical fidelity by adapting the partial differential equation to the choice of discretization by virtue of potentials and gauges. Finite element models engendered by this combination are plagued by non-physical modes that tend to pollute transient and static solutions. The second approach takes a different route and tries to achieve physical fidelity in the simulation by adapting the discretization choice to the partial differential equation. This gives rise to finite element models in which non-physical effects are well controlled and selected governing equations can be satisfied exactly by finite element approximations. Ultimately, this approach leads to simulations with superior physics fidelity.

## 1.2 Magnetic diffusion in highly heterogeneous conductors

The relevant governing equations for the electromagnetic field are obtained from the full Maxwell’s equations by neglecting the displacement current<sup>1</sup>. The result is the set of *eddy currents* equations

$$\nabla \times \mathbf{H} = \mathbf{J} \quad \text{in } \Omega \quad (1.1a)$$

$$\nabla \times \mathbf{E} = -\frac{\partial \mathbf{B}}{\partial t} \quad \text{in } \Omega \quad (1.1b)$$

$$\nabla \cdot \mathbf{B} = 0 \quad \text{in } \Omega \quad (1.1c)$$

$$\nabla \cdot \mathbf{J} = 0 \quad \text{in } \Omega, \quad (1.1d)$$

---

<sup>1</sup>This amounts to neglecting high frequency speed-of-light time scale electromagnetic waves in a conducting medium.



where  $\mathbf{H}$  is the magnetic field,  $\mathbf{J}$  is the current density,  $\mathbf{E}$  is the electric field, and  $\mathbf{B}$  is the magnetic flux density. Initial values of  $\mathbf{B}$  are required to satisfy (1.1c). The system (1.1a)–(1.1d) is closed by adding the constitutive relations

$$\mathbf{B} = \mu\mathbf{H} \quad \text{and} \quad \mathbf{J} = \sigma\mathbf{E} \quad (1.2)$$

where  $\sigma$  and  $\mu$  denote conductivity and permeability of the media, respectively, and appropriate boundary conditions. Here we consider *Type I* conditions

$$\mathbf{n} \times \mathbf{E} = \mathbf{n} \times \mathbf{E}_b \quad \text{and} \quad \mathbf{n} \cdot \mathbf{B} = \mathbf{n} \cdot \mathbf{B}_b \quad \text{on } \Gamma^* \quad (1.3)$$

and *Type II* conditions

$$\mathbf{n} \times \mathbf{H} = \mathbf{n} \times \mathbf{H}_b \quad \text{and} \quad \mathbf{n} \cdot \mathbf{J} = \mathbf{n} \cdot \mathbf{J}_b \quad \text{on } \Gamma. \quad (1.4)$$

posed on disjoint parts  $\Gamma$  and  $\Gamma^*$  of the boundary  $\partial\Omega^2$ .

While the eddy current equations (1.1a)–(1.1d) are a well-known and studied model, using it as a component of the larger Z-pinch model brings up some specific modeling and computational issues. First, implosion of the wire array is accompanied by state transitions from solid to melt and finally, plasma states during which conductivity changes over several ranges of magnitude. As a result, unlike in conventional applications of the eddy current model, here conducting and non-conducting regions are not separated by a static interface. This forces consideration of the eddy current equations on a single, but highly heterogeneous, conductor as the only acceptable modeling choice. Therefore, for us  $\Omega$  will represent a single conducting region in  $\mathbf{R}^3$  with non-constant conductivity  $\sigma$  and permeability  $\mu$  such that

$$0 < \sigma_{\min} \leq \sigma(\mathbf{x}, t) \leq \sigma_{\max} \quad \forall \mathbf{x} \in \Omega \quad (1.5)$$

$$0 < \mu_{\min} \leq \mu(\mathbf{x}, t) \leq \mu_{\max} \quad \forall \mathbf{x} \in \Omega. \quad (1.6)$$

However, no particular smoothness of  $\sigma$  and  $\mu$  can be assumed, i.e., they can be discontinuous functions.

To deliver robust, 3D fully integrated Z-pinch calculations, finite element simulation of the magnetic diffusion must also maintain high fidelity to the underlying physics both at the ideal MHD limit  $\sigma \rightarrow \infty$ , as well as at the highly diffusive limit  $\sigma \rightarrow 0$ . In addition, an efficient solution method for the discrete equations must be available.

In the magnetohydrodynamics modeling literature a great deal of attention is paid to enforcement of equation (1.1c) in the numerical approximation either exactly or to some interpolation error (Toth, [29]). Here we discuss a modeling approach in which equation (1.1c) is satisfied exactly to machine precision and it is desirable to maintain this exactness throughout the magnetohydrodynamics algorithm which must include  $\mathbf{J} \times \mathbf{B}$  forces, Joule heating and an appropriate treatment of magnetic induction in moving media.

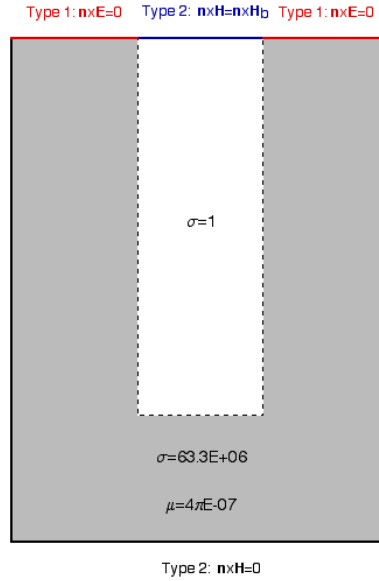
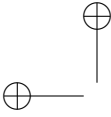


Figure 1.1. Model problem in two-dimensions

### 1.2.1 A two-dimensional model problem

To compare and contrast different finite element methods we further restrict attention to a two-dimensional model problem derived from a setting related to the Z-pinch problem. The region  $\Omega$  is a  $0.003m \times 0.004m$  rectangle. A low conductivity region occupies a slot in the middle of the rectangle that is  $0.003m$  deep and  $0.001m$  wide; see Figure 1.1. We set  $\mu = 4\pi \times 10^{-7}$  in the whole region, and

$$\sigma = \begin{cases} 1 & \text{if } 0.001 < x < 0.002 \text{ and } 0.001 < y < 0.004 \\ 63.3 \times 10^6 & \text{otherwise} \end{cases}$$

The governing equations are obtained from (1.1a)-(1.1d) by the ansatz

$$\mathbf{H} = H_z \mathbf{k} \quad \text{and} \quad \mathbf{E} = E_x \mathbf{i} + E_y \mathbf{j}.$$

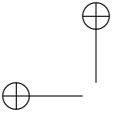
The model problem is driven by a combination of Type I and Type II boundary conditions. Type II boundary consists of the center slot on the top side, the bottom side and the left and right sides of  $\Omega$ . Type I boundary is the complement of Type II; see Figure 1.1. On Type I we prescribe homogeneous tangential  $\mathbf{E}$ :

$$\mathbf{n} \times \mathbf{E} = 0 \quad \text{on } y = 0.004 \text{ and } 0 < x < 0.001 \text{ or } 0.002 < x < 0.003.$$

The tangential magnetic field is set to one at the center slot and zero elsewhere:

$$\mathbf{n} \times \mathbf{H} = \begin{cases} 1 & \text{on } 0.001 < x < 0.002, y = 0.004 \\ 0 & \text{all other parts of Type II boundary} \end{cases}$$

<sup>2</sup>Note that (1.1a) and (1.1b) imply consistency between tangential and normal boundary conditions in each pair.



Based on the domain geometry and the choices of  $\sigma$  and  $\mu$  the steady state<sup>3</sup> will be reached at  $t_{steady} \approx 50 \times 10^{-6}$  sec. In the static limit  $\mathbf{B}$  represents a “tent”-like shape that is flat above the slot and fills the rest of the region.

## 1.3 Vector potential approaches

Nodal spaces have been in the arsenal of finite elements since the very inception of this powerful method. As such they have gained tremendous following and popularity. In large part this is owed to their simplicity, well-developed approximation theory and the fact that nodal elements lead to algebraic problems with well-understood properties and structure. Nevertheless, if applied directly to our model problem they fail to ensure solenoidal approximation of the magnetic flux  $\mathbf{B}$ .

To resolve this problem adherents of nodal elements substitute the original eddy current model (1.1a)–(1.1d) by a set of equations based on a vector magnetic potential in conducting regions and a scalar<sup>4</sup> magnetic potential in all other parts of  $\Omega$ , see e.g., [3, 4]. However, the lack of static interface in our application makes the use of two potentials prohibitively complex for implementation. In this case one introduces a “fudged” void conductivity and considers a single vector magnetic potential for the whole region. Since in conductors  $\nabla \cdot \mathbf{B} = 0$  we must have that  $\mathbf{B} = \nabla \times \mathbf{A}$  in  $\Omega$ . From the Faraday’s law (1.1b)  $\mathbf{E} = -(\frac{\partial \mathbf{A}}{\partial t} + \nabla \phi)$ , where  $\phi$  is a scalar electric potential. In combination with (1.2) and (1.1a) this gives

$$\nabla \times \frac{1}{\mu} \nabla \times \mathbf{A} = -\sigma \left( \frac{\partial \mathbf{A}}{\partial t} + \nabla \phi \right). \quad (1.7)$$

To use the vector potential equation (1.7) one must choose a gauge, i.e., augment it by additional equations and boundary conditions. The Coulomb gauge  $\nabla \cdot \mathbf{A} = 0$  is hard to satisfy numerically by nodal elements and must be added implicitly to the formulation which creates a cascading effect of adding more and more equations; see [3]. Another choice is the Lorenz gauge  $\nabla \cdot \mathbf{A} = -\mu\sigma\phi$ ; see [14, 15, 16]. For homogeneous conductors this gauge is equivalent to the Coulomb gauge; see [4], while for heterogeneous materials it leads to nonsymmetric weak problems and is avoided. In what follows we consider finite element solution of the magnetic diffusion model by two other vector potential formulations that circumvent these problems. However, we will see that other, more serious problems concerning fidelity of the results appear.

### 1.3.1 Modified vector potential formulation

In the *modified vector magnetic potential* formulation of Emson and Simkin [19], the electric potential  $\phi$  is eliminated from (1.7) by the integral transformation

$$\mathbf{A}^* = \mathbf{A} + \int_0^t \nabla \phi dt. \quad (1.8)$$

<sup>3</sup>The value  $\sigma = 63.3 \times 10^6$  gives the nominal conductivity for solid copper. The time scale for magnetic diffusion in solid copper is estimated from  $\mu\sigma L^2$  where  $L$  is characteristic length.

<sup>4</sup>In conventional applications of the eddy current model this has the added benefit of reducing the number of unknowns in void regions.

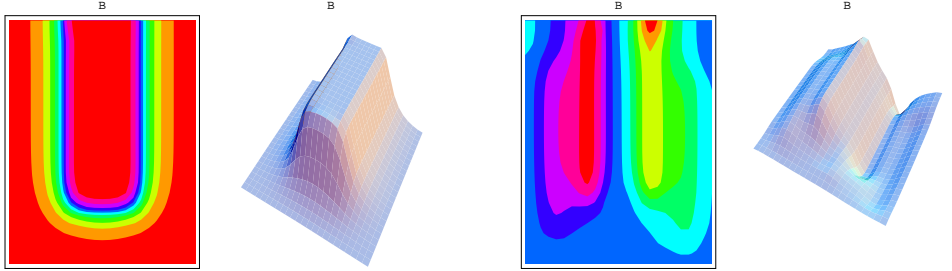
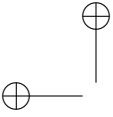


**Figure 1.2.**  $\mathbf{B}$  computed from (1.9):  $t_1$  and  $t_{steady}$ .

The modified potential  $\mathbf{A}^*$  has the property that  $\nabla \times \mathbf{A}^* = \nabla \times \mathbf{A}$  and  $\frac{\partial \mathbf{A}^*}{\partial t} = \frac{\partial \mathbf{A}}{\partial t} + \nabla \phi$  and, as a result, (1.7) can be replaced by

$$\nabla \times \frac{1}{\mu} \nabla \times \mathbf{A}^* + \sigma \frac{\partial \mathbf{A}^*}{\partial t} = 0 \quad \text{in } \Omega. \quad (1.9)$$

This equation is augmented by the boundary conditions

$$\frac{1}{\mu} \nabla \times \mathbf{A} \times \mathbf{n} = \mathbf{H}_b \times \mathbf{n} \quad \text{on Type II} \quad \text{and} \quad \mathbf{n} \times \mathbf{A} = 0 \quad \text{on Type I}, \quad (1.10)$$

derived from the original boundary conditions (1.3)–(1.4) specialized to the model problem in §1.2.1.

Figure 1.2 shows  $\mathbf{B}$  computed from a finite element solution of (1.9)–(1.10) by bilinear nodal elements defined on rectangles. The plot on the left side gives  $\mathbf{B}$  after one time step when it represents the magnetic flux fairly well. The other plot shows the steady state of  $\mathbf{B}$ . Unfortunately, this plot does not capture the correct behavior of  $\mathbf{B}$  at all.

### 1.3.2 Modified Lorenz gauge formulation

Modifications of the Lorenz gauge which give symmetric weak problems for heterogeneous conductors were suggested in [6] and in [11]. The gauge considered in [6] adds the equation

$$\nabla \cdot \sigma \mathbf{A} = -\mu \sigma^2 \phi \quad \text{in } \Omega \quad (1.11)$$

and the boundary conditions

$$\phi = 0 \quad \text{on Type I} \quad \text{and} \quad \mathbf{A} \cdot \mathbf{n} = \kappa^2 \mu \sigma l \phi \quad \text{on Type II} \quad (1.12)$$

to (1.7). The electric potential  $\phi$  can be eliminated from the gauged system which reduces the set of differential equations to:

$$\nabla \times \frac{1}{\mu} \nabla \times \mathbf{A} + \sigma \frac{\partial \mathbf{A}}{\partial t} - \sigma \nabla \left( \frac{1}{\mu \sigma^2} \nabla \cdot \sigma \mathbf{A} \right) = 0 \quad \text{in } \Omega. \quad (1.13)$$

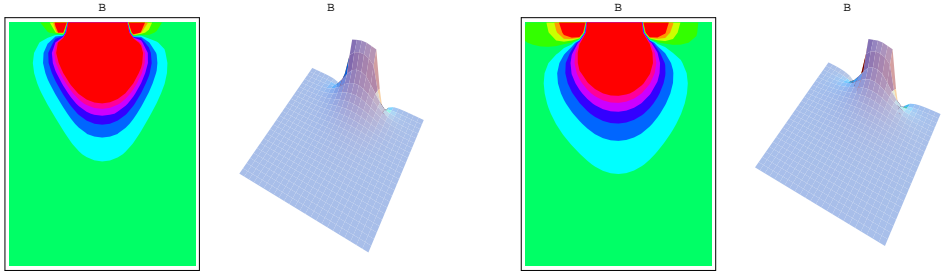
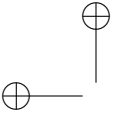


**Figure 1.3.**  $\mathbf{B}$  computed from (1.13):  $t_1$  and  $t_{steady}$ .

For the model problem in §1.2.1 (1.13) is closed by (1.10) augmented with  $\mathbf{A} \cdot \mathbf{n} = 0$  on Type II boundaries.

Figure 1.3 shows approximations of  $\mathbf{B}$  after one time step and its steady state computed from bilinear finite element solution of (1.13). Compared with the solution by modified vector formulation (1.7) now even the first time step is not represented well by the approximation. In fact, behavior of  $\mathbf{B}$  closely resembles that of a *locked* finite element solution.

### 1.3.3 Pitfalls of nodal discretizations

To understand why the two vector potential formulations behave in this unsatisfactory way let us take a look at the equations used to advance the finite element solution in time. We assume that  $\mathbf{A}$  is approximated by a standard  $C^0$  nodal finite element space  $\mathbf{X}^h$  constrained by an appropriate set of boundary conditions. The semidiscrete problem is

$$\mathbf{M}_\sigma \dot{\mathbf{A}}^h + \mathbf{K}_\mu \mathbf{A}^h = \mathbf{f} \quad (1.14)$$

where  $\mathbf{M}_\sigma = (\mathbf{A}^h, \hat{\mathbf{A}}^h)$  is the mass matrix and

$$\mathbf{K}_\mu = \begin{cases} (\frac{1}{\mu} \nabla \times \mathbf{A}^h, \nabla \times \hat{\mathbf{A}}^h) & \text{for (1.9)} \\ (\frac{1}{\mu} \nabla \times \mathbf{A}^h, \nabla \times \hat{\mathbf{A}}^h) + (\nabla \cdot \sigma \mathbf{A}^h, \nabla \cdot \sigma \hat{\mathbf{A}}^h) & \text{for (1.13)} \end{cases}$$

is a stiffness matrix. The qualitative behavior of the solutions in (1.14) depends on the eigenpairs  $(\lambda, \mathbf{x}_\lambda)$  of the generalized eigenvalue problem

$$(\lambda \mathbf{M}_\sigma + \mathbf{K}_\mu) \mathbf{x}_\lambda = 0. \quad (1.15)$$

Consider first (1.15) with  $\mathbf{K}_\mu$  corresponding to the modified formulation (1.9). Figure 1.4 shows the eigenvalues of (1.15) superimposed with the eigenvalues of the discrete curl operator  $\mathbf{C}_\mu = (\frac{1}{\mu} \nabla \times \mathbf{A}^h, \nabla \times \hat{\mathbf{A}}^h)$ . The continuous counterpart of this operator has an infinite dimensional nullspace. However, for the example considered here  $\mathbf{C}_\mu$  turns out to be nonsingular and the zero frequency is approximated by a cluster of small eigenvalues, visible at the bottom left corner of Figure 1.4. The nonsingularity of  $\mathbf{C}_\mu$ , which at first seems counterintuitive, is in fact caused by the

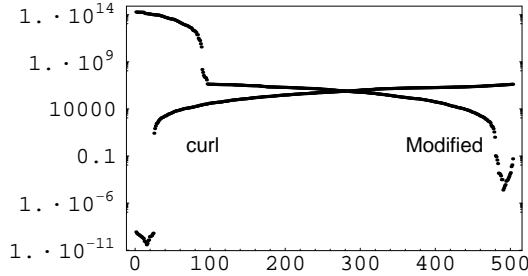


**Figure 1.4.** *Eigenvalues of  $\mathbf{C}_\mu$  and (1.15).*

use of nodal elements to form this matrix. Indeed, in order for  $\mathbf{C}_\mu$  to be singular, the nodal space  $\mathbf{X}^h$  must contain exact gradients. This amounts to the existence of another finite element space  $X^h$ , defined with respect to the same triangulation  $\mathcal{T}_h$ , and such that  $\nabla q^h \in \mathbf{X}^h$  for some  $q^h \in X^h$ . Therefore,  $X^h$  must contain scalar piecewise polynomial functions of one degree higher than those in  $\mathbf{X}^h$ , and whose gradients are  $C^0$  functions. It doesn't take long to see that when  $\mathbf{X}^h$  is constrained by (1.10) such  $X^h$  does not exist; see also [10].

Thus, instead of exact gradients,  $\mathbf{X}^h$  contains vector fields that are “almost gradients”. These fields are further transformed into spurious modes of (1.15) where they cause the nonphysical magnetic flux computed from (1.9). To test this hypothesis let us conduct a simple numerical experiment in which at each time step the finite element vector potential  $\mathbf{A}^h$  is projected onto the orthogonal complement of the spurious modes. For the purpose of this experiment let us deem as “spurious” the modes of (1.15) corresponding the eigenvalue cluster<sup>5</sup> near the origin; see Figure 1.4. Figure 1.5 compares the original finite element solution from (1.9) with a magnetic flux density obtained from our experiment. After the first time step both solutions, shown on the left hand side of Figure 1.5, are indistinguishable. When the original solution reaches its unphysical steady state, the projected solution is still evolving, however, it represents better the desired “tent”-like shape of the exact steady state for  $\mathbf{B}$ . An immediate conclusion that can be drawn from this experiment is that elimination of the modes deemed as “spurious” did improve the transient solution but still left it far from perfect. Thus, there must be more spurious modes left among the ones we deemed as “physical”. Therefore, it seems that all that is needed in order to obtain satisfactory  $\mathbf{B}$  is to identify the remaining spurious modes and purge them from the transient solution.

Unfortunately, this course of action is hardly prudent because, depending on the nodal basis used, spurious modes may remain clustered around the zero frequency, or they may pollute the whole spectrum. Even worse, when  $\mathcal{T}_h$  is refined new spurious modes continue to enter the spectrum from above; see [1], or [7]. This

<sup>5</sup>For the triangulation used in this experiment  $M_\sigma$  and  $K_\mu$  are  $503 \times 503$  matrices. The largest 479 modes of (1.15) were taken as “physical”, while the smallest 24 were the “spurious”.

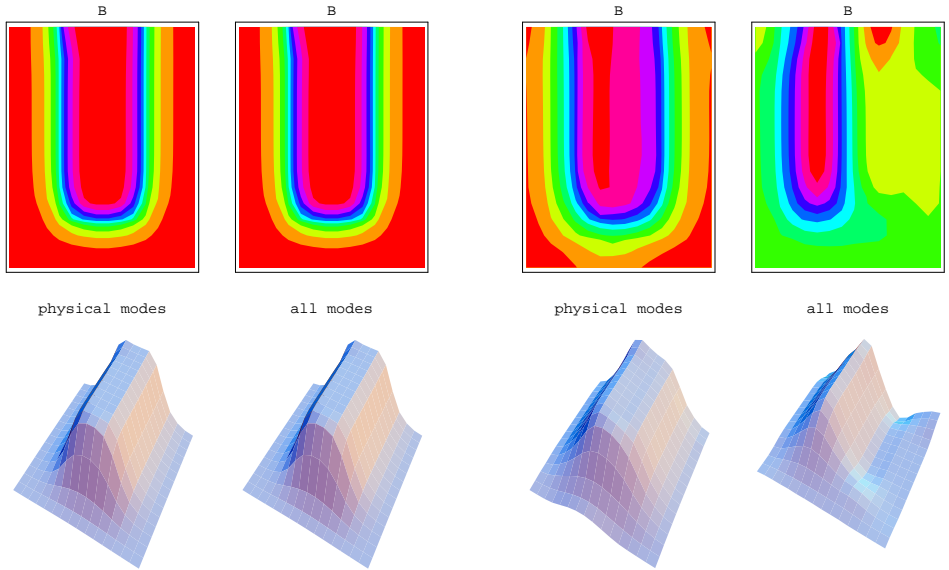


**Figure 1.5.** “Physical” vs. “spurious” approximations of  $\mathbf{B}$ :  $t_1$  and  $t_{steady}$ .

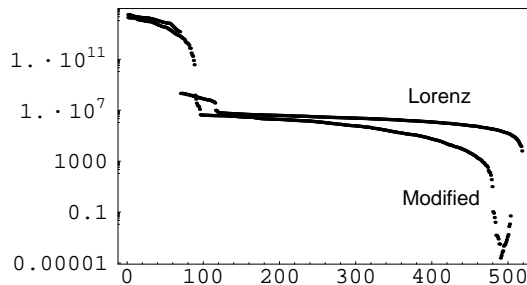


**Figure 1.6.** Eigenvalues of (1.15) for (1.9) and (1.13).

is why we placed “spurious” and “physical” in quotes, and why the experiment conducted above cannot be extended to a practical algorithm.

Let us now consider (1.15) when  $\mathbf{K}_\mu$  includes the contribution from the modified Lorenz gauge, i.e., the case of (1.13). Figure 1.6 shows the new eigenvalues superimposed with the earlier set of eigenvalues corresponding to (1.9). It is clear that the effect of the modified Lorenz gauge is to push the eigenvalues to a higher part of the spectrum. The same effect has been observed in penalty formulations; see [23] and [27]. In other words, the Lorenz gauge (1.11)–(1.12) acts as a penalty term. This explains the “locked” solution phenomena in Figure 1.3: since the spectrum is pushed up, the only modes that it contains are fast transients relative to



the time scale of the model problem. These transients quickly die out, leaving us with a solution “frozen” at an unphysical state.

## 1.4 Matching physics with discretization

It is very unlikely that a finite dimensional approximation of a process taking place in an infinite dimensional space can avoid “non-physical” effects. Thus, by themselves, spurious modes are only part of the problem experienced by the two vector potential formulations. The main culprit for the poor performance of (1.9) and (1.13) is that nodal bases are incapable of providing discrete problems in which nonphysical modes are confined to the zero frequency. Without this property transient and static solutions will inevitably become polluted by these modes; see [18].

Alternatively, we can view these difficulties as stemming from inadequate approximation of the kernel of the curl operator by nodal elements; see [10]. As a result, a remedy can be sought by using finite element spaces which contain a sufficiently large supply of gradients. To find such spaces we turn attention to the mathematical structure of the Maxwell’s equations which is closely related to the notions of exactness and De Rham complex; see, e.g., [9]–[10], and [21].

### 1.4.1 De Rham complex

The domains of the gradient, curl and divergence, relative to  $\Gamma$  are

$$H_0(\Omega, \mathbf{grad}) = \{\phi \in H(\Omega, \mathbf{grad}) \mid \phi = 0 \quad \text{on } \Gamma\}, \quad (1.16)$$

$$H_0(\Omega, \mathbf{curl}) = \{\mathbf{u} \in H(\Omega, \mathbf{curl}) \mid \mathbf{u} \times \mathbf{n} = 0 \quad \text{on } \Gamma\}, \quad (1.17)$$

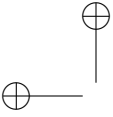
$$H_0(\Omega, \text{div}) = \{\mathbf{u} \in H(\Omega, \text{div}) \mid \mathbf{u} \cdot \mathbf{n} = 0 \quad \text{on } \Gamma\}, \quad (1.18)$$

where  $H(\Omega, \mathbf{grad})$ ,  $H(\Omega, \mathbf{curl})$ , and  $H(\Omega, \text{div})$  denote spaces of square integrable functions whose gradients, curls and divergences are also square integrable. As usual, the space of all square integrable functions on  $\Omega$  is denoted by  $L^2(\Omega)$ . The four spaces  $H_0(\Omega, \mathbf{grad})$ ,  $H_0(\Omega, \mathbf{curl})$ ,  $H_0(\Omega, \text{div})$ ,  $L^2(\Omega)$  and the three operators  $\nabla$ ,  $\nabla \times$  and  $\nabla \cdot$  form a *De Rham complex relative to  $\Gamma$* . The dual De Rham complex is defined relative to  $\Gamma^*$  and involves the adjoint operators  $\nabla^*$ ,  $(\nabla \times)^*$  and  $(\nabla \cdot)^*$ .

A fundamental property of De Rham’s complex is that each differential operator maps its domain into the kernel of the next differential operator. A combination of spaces and operators with such property is called *exact sequence*. Symbolically, the exactness property is represented by the following diagram:

$$H_0(\Omega, \mathbf{grad}) \xrightarrow{\nabla} H_0(\Omega, \mathbf{curl}) \xrightarrow{\nabla \times} H_0(\Omega, \text{div}) \xrightarrow{\nabla \cdot} L^2(\Omega). \quad (1.19)$$

The importance of (1.19) stems from the fact that Maxwell’s equations can be



described in terms of a *Tonti* diagram built upon this complex; see [10]:

	<i>Ampere</i>		<i>Faraday</i>
$H_0(\Omega, \mathbf{grad})$	$\psi$		$0$
$\nabla$	$\downarrow$		$\uparrow$
$H_0(\Omega, \mathbf{curl})$	$\mathbf{H}$	$\Rightarrow \mu \mathbf{H} = \mathbf{B} \Rightarrow$	$\mathbf{B}$
$\nabla \times$	$\downarrow$		$\uparrow$
$H_0(\Omega, \mathbf{div})$	$\mathbf{J}$	$\Leftarrow \mathbf{J} = \sigma \mathbf{E} \Leftarrow$	$\mathbf{E}$
$\nabla \cdot$	$\downarrow$		$\uparrow$
$L_0^2(\Omega)$	$0$		$\phi$
			$H_0^*(\Omega, \mathbf{grad})$

(1.20)

### 1.4.2 Discrete De Rham complex

How can the Tonti diagram help us devise a better finite element method for the magnetic diffusion problem? The diagram (1.20) represents a mathematical abstraction of the physics that governs electromagnetic phenomena. As such it reveals the intrinsic structure of Maxwell’s equations responsible for the qualitative behavior of their solutions. To capture this behavior, a finite element solution must evolve from a setting that approximates this structure, i.e., a discretization that approximates both the spaces in (1.20) and the relations between them induced by the gradient, curl and divergence operators. In short, we seek four finite element spaces  $\mathcal{W}^i$ ,  $i = 0, \dots, 3$  that are subspaces of  $H_0(\Omega, \mathbf{grad})$ ,  $H_0(\Omega, \mathbf{curl})$ ,  $H_0(\Omega, \mathbf{div})$ , and  $L^2(\Omega)$ , respectively, and which form an exact sequence, that is

$$\mathcal{W}^0 \xrightarrow{\nabla} \mathcal{W}^1 \xrightarrow{\nabla \times} \mathcal{W}^2 \xrightarrow{\nabla \cdot} \mathcal{W}^3. \tag{1.21}$$

Then a discrete model of (1.1a)–(1.1d) can be derived from (1.20) by substituting the function spaces by the finite element spaces  $\mathcal{W}^i$ , an idea originally suggested in [8], [9].

In this section we will develop the desired exact sequence of finite elements for general unstructured hexahedral and quadrilateral grids. The progenitor of this exact sequence is the original hexahedral “edge” element developed by van Welij [32]. For parallelepipeds and parallelograms some spaces in the exact sequence will coincide with the well-known Nedelec, and BDFM ( Brezzi, Douglas, Fortin and Marini) spaces; see [24], [25], [13], and [17]. However, for general hexahedral/quadrilateral grids the elements in our sequence are different in the sense that they are not an affine<sup>6</sup> family of finite element spaces (see [12, p. 72]).

#### Exact sequence on hexahedral grids

We consider  $\mathbf{R}^3$  endowed with a physical coordinate frame  $(x_1, x_2, x_3) \equiv \mathbf{x}$  and a parameter (reference) frame  $(\xi_1, \xi_2, \xi_3) \equiv \boldsymbol{\xi}$ . In what follows the indices  $\alpha, \beta$  and  $\gamma$

<sup>6</sup>A general method for developing affine families of exact sequences can be found in [21]. Curvilinear hexahedral triangulations are considered in [30].

take the values  $\pm 1$  and the indices  $i, j, k$  form an even permutation of the numbers  $1, 2, 3$ .

Let  $\hat{K}$  denote the open cube  $(-1, 1)^3$  in the reference space and let  $K$  be a non-degenerate, convex hexahedral in the physical space with vertices  $\mathbf{x}^{\alpha\beta\gamma}$ ,  $\alpha, \beta, \gamma = \pm 1$ . Furthermore, let  $Q_1(\hat{K})$  denote the space of all polynomials defined on  $\hat{K}$  whose degree does not exceed one in each coordinate direction. Let  $\hat{\phi}_i^\alpha(\boldsymbol{\xi}) = \frac{1}{2}(1 + \alpha\xi_i)$  and define the function  $\mathbf{F} = (F_1, F_2, F_3) \in Q_1(\hat{K})$

$$\mathbf{F}(\boldsymbol{\xi}) = \sum_{\alpha, \beta, \gamma = \pm 1} \mathbf{x}^{\alpha\beta\gamma} \hat{\phi}_1^\alpha(\boldsymbol{\xi}) \hat{\phi}_2^\beta(\boldsymbol{\xi}) \hat{\phi}_3^\gamma(\boldsymbol{\xi}). \quad (1.22)$$

The nodes, the edges and the faces of  $\hat{K}$  can be expressed as

$$\begin{aligned} \boldsymbol{\xi}^{\alpha\beta\gamma} &= \{\xi_i = \alpha, \xi_j = \beta, \xi_k = \gamma\} \\ \boldsymbol{\xi}_{ij}^{\alpha\beta} &= \{\xi_i = \alpha, \xi_j = \beta, -1 \leq \xi_k \leq 1\} \\ \boldsymbol{\xi}_i^\alpha &= \{\xi_i = \alpha, -1 \leq \xi_j, \xi_k \leq 1\}. \end{aligned}$$

Let  $\mathbf{x}^{\alpha\beta\gamma}$ ,  $\mathbf{x}_{ij}^{\alpha\beta}$  and  $\mathbf{x}_i^\alpha$  denote the nodes, the edges and the faces of  $K$ . Then, it is not difficult to see that  $\mathbf{F}$  is the unique invertible mapping between  $\hat{K}$  and  $K$  with the property  $\mathbf{x}^{\alpha\beta\gamma} = \mathbf{F}(\boldsymbol{\xi}^{\alpha\beta\gamma})$ ,  $\mathbf{x}_{ij}^{\alpha\beta} = \mathbf{F}(\boldsymbol{\xi}_{ij}^{\alpha\beta})$ , and  $\mathbf{x}_i^\alpha = \mathbf{F}(\boldsymbol{\xi}_i^\alpha)$ . Let  $\mathbf{G} \equiv (G_1, G_2, G_3) : K \mapsto \hat{K}$  denote the inverse of  $\mathbf{F}$  and let  $J_{\mathbf{F}} = (V_1, V_2, V_3)$  and  $J_{\mathbf{G}} = (\nabla G_1, \nabla G_2, \nabla G_3)^T$ , where  $V_i = (\partial F_1 / \partial \xi_i, \partial F_2 / \partial \xi_i, \partial F_3 / \partial \xi_i)^T$ , denote the Jacobians of the two mappings. A simple calculation reveals that  $\det J_{\mathbf{F}} = V_i \cdot (V_j \times V_k)$  and  $\det J_{\mathbf{G}} = \nabla G_i \cdot (\nabla G_j \times \nabla G_k)$ , while from  $(\mathbf{F} \circ \mathbf{G})(\mathbf{x}) = \mathbf{x}$  it follows that

$$V_i \cdot \nabla G_j = \delta_{ij}. \quad (1.23)$$

Solving (1.23) for  $V_i$  and  $\nabla G_j$  gives

$$V_i = (\nabla G_j \times \nabla G_k) \det J_{\mathbf{F}} \quad \text{and} \quad \nabla G_i = (V_j \times V_k) \det J_{\mathbf{G}} \quad (1.24)$$

The unit normal to a face  $\mathbf{x}_i^\alpha$  and the unit tangent to an edge  $\mathbf{x}_{ij}^{\alpha\beta}$  are given by

$$\mathbf{n} = \frac{\nabla G_i}{\|\nabla G_i\|} \quad \text{and} \quad \mathbf{t} = \frac{(\nabla G_i \times \nabla G_j)}{\|\nabla G_i \times \nabla G_j\|} \quad (1.25)$$

respectively. Changing variables in (1.25) and using (1.24) shows that the corresponding vector fields on  $\hat{K}$  are

$$(\mathbf{n} \circ \mathbf{F}) = \frac{V_j \times V_k}{\|(V_j \times V_k)\|} \quad \text{and} \quad (\mathbf{t} \circ \mathbf{F}) = \frac{V_k}{\|V_k\|}, \quad (1.26)$$

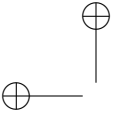
respectively. Let  $\phi_i^\alpha(\mathbf{x}) = \hat{\phi}_i^\alpha(\mathbf{G}(\mathbf{x})) \equiv \frac{1}{2}(1 + \alpha G_i(\mathbf{x}))$ . We consider four sets of functions defined on  $K$  as follows:

$$W_{ijk}^{\alpha\beta\gamma} = \phi_i^\alpha \phi_j^\beta \phi_k^\gamma \quad (1.27a)$$

$$W_{ij}^{\alpha\beta} = \phi_i^\alpha \phi_j^\beta \nabla \phi_k^\gamma \quad (1.27b)$$

$$W_i^\alpha = \phi_i^\alpha (\nabla \phi_j^\beta \times \nabla \phi_k^\gamma) \quad (1.27c)$$

$$W = \nabla \phi_i^\alpha \cdot (\nabla \phi_j^\beta \times \nabla \phi_k^\gamma). \quad (1.27d)$$



These sets span four spaces denoted by  $\mathcal{W}^0(K)$ ,  $\mathcal{W}^1(K)$ ,  $\mathcal{W}^2(K)$  and  $\mathcal{W}^3(K)$ , respectively. Fundamental properties of (1.27a)–(1.27d) are associated with the “nodes”, “edges”, and “faces” of  $K$ . The “point” mass of the scalar functions in (1.27a) is

$$\int_K W_{ijk}^{\alpha\beta\gamma}(\mathbf{x}) \cdot \delta(\mathbf{x}^{\kappa\mu\nu}) d\mathbf{x} = \begin{cases} 1 & \text{if } \mathbf{x}^{\kappa\mu\nu} = \mathbf{x}^{\alpha\beta\gamma} \\ 0 & \text{at all other nodes} \end{cases}.$$

Thus,  $\mathcal{W}^0(K)$  is a “nodal” space with basis  $\{W_{ijk}^{\alpha\beta\gamma}\}$ . The circulations of the vector fields in (1.27b) are

$$\int_{\mathbf{x}_{st}^{\kappa\mu}} W_{ij}^{\alpha\beta}(\mathbf{x}) \cdot \mathbf{t} dl = \begin{cases} 1 & \text{if } \mathbf{x}_{st}^{\kappa\mu} = \mathbf{x}_{ij}^{\alpha\beta} \\ 0 & \text{along all other edges} \end{cases}.$$

so we call  $W_{ij}^{\alpha\beta}$  an “edge” basis and  $\mathcal{W}^1(K)$  an edge space. The vector fields in (1.27c) have a similar property with respect to their fluxes across the faces of  $K$ :

$$\int_{\mathbf{x}_s^\kappa} W_i^\alpha(\mathbf{x}) \cdot \mathbf{n} dS = \begin{cases} 1 & \text{if } \mathbf{x}_s^\kappa = \mathbf{x}_i^\alpha \\ 0 & \text{all other faces} \end{cases}.$$

Thus,  $W_i^\alpha$  is a “face” basis and  $\mathcal{W}^2(K)$  is a face space. Lastly,

$$\int_K W(\mathbf{x}) d\mathbf{x} = 1.$$

so  $W$  is a “volume” basis and  $\mathcal{W}^3(K)$  is a volume space. Degrees of freedom (DOF) for  $\mathcal{W}^0(K)$  are “point masses”, or simply the nodal values of a scalar function. The DOFs for  $\mathcal{W}^1(K)$  are circulations of a vector field along the edges of  $K$ , the DOFs for  $\mathcal{W}^2(K)$  are fluxes across the faces, and the sole DOF for  $\mathcal{W}^3(K)$  is the total mass of  $K$  for a given scalar density function. Lastly, using the chain rule, elementary vector calculus identities and (1.27a)–(1.27d) it can be shown that

$$\begin{aligned} \nabla W_{ijk}^{\alpha\beta\gamma} &= \sigma_{ij} W_{ij}^{\alpha\beta} + \sigma_{jk} W_{jk}^{\beta\gamma} + \sigma_{ki} W_{ki}^{\gamma\alpha} \\ \nabla \times W_{ij}^{\alpha\beta} &= \sigma_i W_i^\alpha + \sigma_j W_j^\beta \\ \nabla \cdot W_i^\alpha &= \sigma W, \end{aligned}$$

for some  $\{\sigma_{ij}, \sigma_i, \sigma\} \in \{\pm 1\}$ , i.e., the four spaces  $\mathcal{W}^i(K)$  form an exact sequence that verifies (1.21). After changing variables, and with the help of (1.24), we find a representation of the bases on  $\tilde{K}$ :

$$\begin{aligned} \hat{W}_{ijk}^{\alpha\beta\gamma} &= \frac{1}{8} (1 + \alpha\xi_i)(1 + \beta\xi_j)(1 + \gamma\xi_k) \\ \hat{W}_{ij}^{\alpha\beta} &= \frac{1}{8 \det \mathbf{J}_{\mathbf{F}}} (1 + \alpha\xi_i)(1 + \beta\xi_j)(V_i \times V_j) \\ \hat{W}_i^\alpha &= \frac{1}{8 \det \mathbf{J}_{\mathbf{F}}} (1 + \alpha\xi_i) V_i \\ \hat{W} &= \frac{1}{8 \det \mathbf{J}_{\mathbf{F}}} \end{aligned}$$

Next consider a triangulation  $\mathcal{T}_h$  of  $\Omega$  into hexahedral finite elements, and let  $\mathcal{W}^i(K)$  denote the sequence on  $K \in \mathcal{T}_h$ . To combine  $\mathcal{W}^i(K)$  into an exact sequence  $\mathcal{W}^i(\Omega)$ , defined with respect to  $\mathcal{T}_h$ , let  $\mathcal{N}$ ,  $\vec{\mathcal{E}}$ ,  $\vec{\mathcal{F}}$  and  $\mathcal{K}$  denote the sets of all nodes, oriented edges, oriented faces, and hexahedrons in  $\mathcal{T}_h$ , respectively. Then we introduce four sets of functions parametrized by  $\mathcal{N}$ ,  $\vec{\mathcal{E}}$ ,  $\vec{\mathcal{F}}$  and  $\mathcal{K}$ , and such that

$$\begin{aligned} \int_{\Omega} W_{\mathcal{N}_i}(\mathbf{x}) \cdot \delta(\mathcal{N}_j) d\mathbf{x} &= \delta_{ij}; & W_{\mathcal{N}_i}|_K &\in \mathcal{W}^0(K) \\ \int_{\vec{\mathcal{E}}_j} W_{\vec{\mathcal{E}}_i}(\mathbf{x}) \cdot \mathbf{t} dl &= \delta_{ij}; & W_{\vec{\mathcal{E}}_i}|_K &\in \mathcal{W}^1(K) \\ \int_{\vec{\mathcal{F}}_j} W_{\vec{\mathcal{F}}_i}(\mathbf{x}) \cdot \mathbf{n} dS &= \delta_{ij}; & W_{\vec{\mathcal{F}}_i}|_K &\in \mathcal{W}^2(K) \\ \int_{\mathcal{K}_j} W_{\mathcal{K}_i}(\mathbf{x}) d\mathbf{x} &= \delta_{ij}; & W_{\mathcal{K}_i}|_K &\in \mathcal{W}^0(K) \end{aligned}$$

The sets  $\{W_{\mathcal{N}}\}$ ,  $\{W_{\vec{\mathcal{E}}}\}$ ,  $\{W_{\vec{\mathcal{F}}}\}$ , and  $\{W_{\mathcal{K}}\}$  span the spaces  $\mathcal{W}^i(\Omega)$ . The space  $\mathcal{W}^0(\Omega)$  is  $H(\Omega, \mathbf{grad})$  conforming because it contains continuous functions. Definition of  $W_{\vec{\mathcal{E}}}$  and (1.25) imply that  $\mathcal{W}^1(\Omega)$  contains vector fields that are tangentially continuous along the edges in  $\vec{\mathcal{E}}$ . Therefore, this space is  $H(\Omega, \mathbf{curl})$  conforming. Likewise,  $\mathcal{W}^2(\Omega)$  contains fields that are normally continuous across the faces  $\vec{\mathcal{F}}$ . This makes  $\mathcal{W}^2(\Omega)$   $H(\Omega, \mathbf{div})$  conforming. Clearly,  $\mathcal{W}^3(\Omega) \subset L^2(\Omega)$ . Exactness of this sequence follows easily from the exactness of the element spaces  $\mathcal{W}^i(K)$ .

### Exact sequence on quadrilateral grids

For quadrilateral triangulations  $\mathcal{T}_h$  of planar regions  $\Omega$ , an “exact” sequence can be derived by proper restriction of a sequence defined on hexahedrons extruded from planar finite elements. We use quotes to emphasize that in  $\mathbf{R}^2$  (1.21) must be changed to accommodate the two different planar curl operators.

Given  $K \in \mathcal{T}_h$  the extruded hexahedron is defined by  $\tilde{K} = \{\mathbf{x} | (x_1, x_2) \in K, -1 < x_3 < 1\}$ . As a result,  $F_3(\boldsymbol{\xi}) = \xi_3$ ,  $V_3 = \mathbf{k}$ ,  $\nabla G_3 = \mathbf{k}$ , and (1.24) simplifies to  $\nabla G_1 = (V_2 \times \mathbf{k})/\det J_{\mathbf{F}}$  and  $\nabla G_2 = (\mathbf{k} \times V_1)/\det J_{\mathbf{F}}$ . Inserting these expressions in (1.27a)–(1.27d) yields four pairs of basis function sets on  $K$  and  $\tilde{K}$ :

$$\begin{aligned} W_{ij^*}^{\alpha\beta*} &= \phi_i^\alpha \phi_j^\beta; & \hat{W}_{ij^*}^{\alpha\beta*} &= \frac{1}{4}(1 + \alpha\xi_i)(1 + \beta\xi_j) \\ W_{ij^*}^{\alpha*} &= \phi_i^\alpha \nabla \phi_j^\beta; & \hat{W}_{ij^*}^{\alpha*} &= \frac{1}{4\det J_{\mathbf{F}}}(1 + \alpha\xi_i)(V_j \times \mathbf{k}) \\ W_i^\alpha &= \phi_i^\alpha (\nabla \phi_j^\beta \times \mathbf{k}); & \hat{W}_i^\alpha &= \frac{1}{4\det J_{\mathbf{F}}}(1 + \alpha\xi_i)V_i; \\ W &= \nabla \phi_i^\alpha \cdot (\nabla \phi_j^\beta \times \frac{\mathbf{k}}{2}); & \hat{W} &= \frac{1}{4\det J_{\mathbf{F}}} \end{aligned}$$

By the chain rule

$$\nabla W_{ij^*}^{\alpha\beta*} = \phi_i^\alpha \nabla \phi_j^\beta + \phi_j^\beta \nabla \phi_i^\alpha$$

which is a sum of  $\mathcal{W}^1(K)$  basis functions, and

$$\nabla \cdot W_i^\alpha = \phi_i^\alpha (\nabla \phi_j^\beta \times \mathbf{k})$$

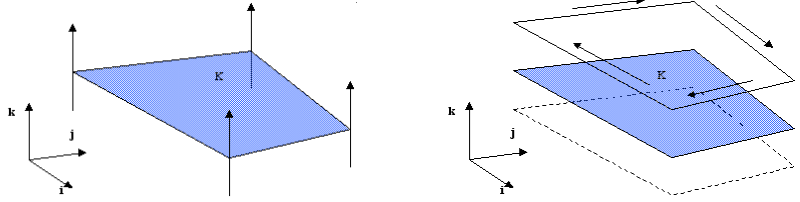
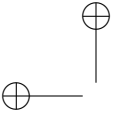


**Figure 1.7.** *Virtual (perpendicular) and parallel edges on  $\tilde{K}$ .*

which is a  $\mathcal{W}^3(K)$  function. Therefore  $\nabla\mathcal{W}^0(K) \subset \mathcal{W}^1(K)$  and  $\nabla \cdot \mathcal{W}^2(K) \subset \mathcal{W}^3(K)$ . The curl relation is a bit more involved as there are two ways to interpret this operator in  $\mathbf{R}^2$ . The first one is to apply curl to vector fields  $\phi\mathbf{k}$  and treat it as an operator that maps scalar functions  $\phi$  into vector fields in the  $(\mathbf{i}, \mathbf{j})$  plane. We use this interpretation when curl is applied to the basis functions  $W_{ij}^{\alpha\beta} = \phi_i^\alpha \phi_j^\beta \frac{\mathbf{k}}{2} = \frac{1}{2} W_{ij*}^{\alpha\beta*} \mathbf{k}$  associated with the four vertical edges of  $\tilde{K}$ ; see Figure 1.7. Then,

$$\nabla \times W_{ij}^{\alpha\beta} = \frac{1}{2} \left( \phi_i^\alpha (\nabla \phi_j^\beta \times \mathbf{k}) + \phi_j^\beta (\nabla \phi_i^\alpha \times \mathbf{k}) \right) = \frac{1}{2} (W_i^\alpha - W_j^\beta)$$

which shows that  $\nabla \times \mathcal{W}^0(K) \subset \mathcal{W}^2(K)$ . A second interpretation of the curl can be derived by applying it to vector fields  $\mathbf{u} = u_1\mathbf{i} + u_2\mathbf{j}$  and treating the result as an operator that maps planar vector fields into scalar functions. We use this interpretation when curl is applied to the basis functions  $W_{i3}^{\alpha+} = \phi_i^\alpha \phi_3^+ \nabla \phi_j^\beta = \phi_i^\alpha \nabla \phi_j^\beta = W_{ij}^{\alpha*}$ , associated with edges on the top face of  $\tilde{K}$ ; see Figure 1.7. Here,

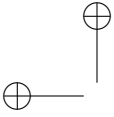
$$\nabla \times \left[ W_{23}^{\alpha+} \right]_{\phi_3^+=1} = \nabla \times \left( \phi_i^\alpha \nabla \phi_j^\beta \right) = \nabla \phi_i^\alpha \times \nabla \phi_j^\beta.$$

which establishes the inclusion  $\mathcal{W}^1(K) \subset \mathcal{W}^3(K)$ . Thus, in two-dimensions (1.21) is modified to

$\mathcal{W}^1$	$\xleftarrow{\nabla}$	$\mathcal{W}^0$	$\xrightarrow{\nabla \times}$	$\mathcal{W}^2$	$\xrightarrow{\nabla \cdot}$	$\mathcal{W}^3$	(1.28)
$\mathcal{W}^1$			$\xrightarrow{\nabla \times}$			$\mathcal{W}^3$	

### 1.4.3 Transient solution using the exact sequence

We will now use the spaces  $\mathcal{W}^i$  to construct a finite element model for the magnetic diffusion. Thanks to the exactness property this discrete model can be easily customized and adapted to different simulation objectives and constitutive hypothesis. For example, if charge conservation (expressed locally by the Ampere’s theorem) is more important than magnetic flux conservation (expressed locally by Faraday’s law), then one can develop a finite element model by taking advantage of the exactness property on the left hand side of (1.20). This was done by Bossavit and Verite in [8] in what constitutes the first example of a discrete Maxwell model built upon



an exact sequence (Whitney forms) of finite element spaces. If, instead, charge and flux conservation are considered to be equally important, then exact sequences can be used on both sides of (1.20), resulting in a model where the constitutive relation (1.2) is enforced weakly.

For us, however, the main objective is to obtain solenoidal approximations of the magnetic flux assuming that (1.2) are valid and true descriptions of the material properties. To meet these criteria we consider a finite element model which takes advantage of the exactness on the right, Faraday's side of (1.20), while the constitutive relation (1.2) is used to eliminate  $\mathbf{H}$  and  $\mathbf{J}$  from the system. This situation is depicted by the discrete Tonti diagram (1.29)

	<i>Ampere</i>		<i>Faraday</i>		
$\mathcal{W}^2$	$\frac{1}{\mu} \mathbf{B}_h$	$\dots$	$\mathbf{B}_h$	$\mathcal{W}^2$	(1.29)
$\nabla \times$	$\vdots$		$\uparrow$	$\nabla \times$	
$\mathcal{W}^1$	$\sigma \mathbf{E}_h$	$\dots$	$\mathbf{E}_h$	$\mathcal{W}^1$	

where

$$\mathbf{B}_h = \sum_{\vec{\mathcal{F}}} \Phi_{\vec{\mathcal{F}}}(t) W_{\vec{\mathcal{F}}}; \quad \mathbf{E}_h = \sum_{\vec{\mathcal{E}}} C_{\vec{\mathcal{E}}}(t) W_{\vec{\mathcal{E}}},$$

are expansions of  $\mathbf{B}_h$  and  $\mathbf{E}_h$  in terms of edge and face basis functions. The discrete magnetic diffusion model then is to find  $(\mathbf{B}_h, \mathbf{E}_h) \in \mathcal{W}^2 \times \mathcal{W}^1$  such that

$$\nabla \times \frac{1}{\mu} \mathbf{B}_h = \sigma \mathbf{E}_h \quad \text{in } \Omega \quad (1.30a)$$

$$\nabla \times \mathbf{E}_h = -\frac{\partial \mathbf{B}_h}{\partial t} \quad \text{in } \Omega \quad (1.30b)$$

$$\mathbf{n} \times \mathbf{E}_h = \mathbf{n} \times \mathbf{E}_b \quad \text{on Type I}; \quad \mathbf{n} \times \frac{1}{\mu} \mathbf{B}_h = \mathbf{n} \times \mathbf{H}_b \quad \text{on Type II.} \quad (1.30c)$$

The finite element problem (1.30a)–(1.30c) requires proper interpretation. The discrete Faraday law (1.30b) holds exactly thanks to the inclusion  $\nabla \times \mathcal{W}^1 \subset \mathcal{W}^2$ . The Ampere's theorem (1.30a) and the boundary condition on Type II segments are, in contrast, interpreted as a weak equation

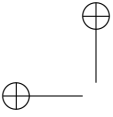
$$\int_{\Omega} \frac{1}{\mu} \mathbf{B}_h \cdot \nabla \times \hat{\mathbf{E}}_h d\Omega + \int_{\Gamma} (\mathbf{n} \times \mathbf{H}_b) \cdot \hat{\mathbf{E}}_h d\Gamma = \int_{\Omega} \sigma \mathbf{E}_h \cdot \hat{\mathbf{E}}_h d\Omega \quad \forall \hat{\mathbf{E}}_h \in \mathcal{W}^1 \quad (1.31)$$

in which the tangential magnetic field is natural boundary condition. This interpretation of (1.30a) is necessitated by the fact that  $\mathcal{W}^2$  is only  $H(\Omega, \text{div})$  conforming and  $\nabla \times \mathbf{B}_h$  does not have a meaning.

To solve our discrete model the time derivative in (1.30b) is replaced by a finite difference leading to a fully discrete, algebraic system for  $\mathbf{E}_h^{n+1}$  and  $\mathbf{B}_h^{n+1}$ :

$$\int_{\Omega} \sigma \mathbf{E}_h^{n+1} \cdot \hat{\mathbf{E}}_h - \frac{1}{\mu} \mathbf{B}_h^{n+1} \cdot \nabla \times \hat{\mathbf{E}}_h d\Omega = \int_{\Gamma} (\mathbf{n} \times \mathbf{H}_b) \cdot \hat{\mathbf{E}}_h d\Gamma \quad \forall \hat{\mathbf{E}}_h \in \mathcal{W}^1 \quad (1.32a)$$

$$-\frac{\mathbf{B}_h^{n+1} - \mathbf{B}_h^n}{\Delta t} = \nabla \times \mathbf{E}_h^{n+1}. \quad (1.32b)$$



The fully discrete model combines a weak Galerkin form of Ampere's law (1.32a) with a finite volume like form of discrete Faraday's law (1.32b). However, (1.32b) is not a finite volume equation because it is based on functional representation of the fields rather than a discrete set of values. As a result, the model considered here gives rise to approximations that are bona fide vector fields rather than a set of discrete quantities defined with respect to a lattice.

To solve (1.32a)-(1.32b) we proceed as follows. Because  $\nabla \times \mathbf{E}_h^{n+1}$  is in  $\mathcal{W}^2$  the second equation can be solved exactly for  $\mathbf{B}_h^{n+1}$ :

$$\mathbf{B}_h^{n+1} = \mathbf{B}_h^n - \Delta t \nabla \times \mathbf{E}_h^{n+1}. \quad (1.33)$$

This expression is substituted in (1.32a) to obtain an equation for  $\mathbf{E}_h^{n+1}$  only:

$$\begin{aligned} & \int_{\Omega} \sigma \mathbf{E}_h^{n+1} \cdot \hat{\mathbf{E}}_h + \frac{\Delta t}{\mu} \left( \nabla \times \mathbf{E}_h^{n+1} \right) \cdot \left( \nabla \times \hat{\mathbf{E}}_h \right) d\Omega \\ &= \int_{\Omega} \frac{1}{\mu} \mathbf{B}_h^n \cdot \left( \nabla \times \hat{\mathbf{E}}_h \right) d\Omega + \int_{\Gamma} \left( \mathbf{n} \times \mathbf{H}_b \right) \cdot \hat{\mathbf{E}}_h d\Gamma \quad \forall \hat{\mathbf{E}}_h \in \mathcal{W}^1. \end{aligned} \quad (1.34)$$

After  $\mathbf{E}_h^{n+1}$  is computed from (1.34) it is used in (1.33) to advance the magnetic flux density to the next time step. Therefore, it is guaranteed that  $\nabla \cdot \mathbf{B}_h^n = 0$  for all  $n > 0$ , provided<sup>7</sup>  $\nabla \cdot \mathbf{B}_h^0 = 0$ .

Another attractive feature of our model is the unprecedented ease with which Type I and Type II boundary conditions can be imposed on the finite element solutions. For example, since the DOF's for  $\mathbf{E}_h$  are the circulations of the electric field along the edges, setting  $\mathbf{n} \times \mathbf{E}_h = 0$  on Type I boundaries amounts to setting all coefficients  $C_{\mathcal{E}}$ , associated with Type I edges, to zero. This situation sharply contrasts with the use of nodal elements where tangential and normal boundary conditions pose a difficult problem.

The efforts expended for the design of the spaces  $\mathcal{W}^i$  and the finite element model (1.30a)–(1.30c) ultimately pay off in exemplary physical fidelity of the numerical simulation. Figure 1.8 shows the initial electric field  $\mathbf{E}$  and magnetic flux density  $\mathbf{B}$  and their steady states obtained from (1.32a)–(1.32b) after 20 time steps with  $\Delta t = 2.5 \times 10^{-6}$  sec. We observe the desired “tent” shape of the steady state magnetic flux density and the correct diffusion time of  $50 \times 10^{-6}$  sec.

In conclusion, let us mention that exact sequences can be used to rehabilitate the modified vector potential formulation (1.9). All that is needed for this purpose is to replace the nodal approximation of  $\mathbf{A}$  with a  $\mathcal{W}^1$  finite element vector field  $\mathbf{A}_h = \sum_{\mathcal{E}} C_{\mathcal{E}}(t) W_{\mathcal{E}}$ . The fully discrete equation for advancing  $\mathbf{A}_h$  in time then looks exactly like (1.34). Similarly, the magnetic flux density approximation  $\mathbf{B}_h = \nabla \times \mathbf{A}_h$  belongs to  $\mathcal{W}^2$  and is always solenoidal. Solutions computed in this manner will be indistinguishable from the solutions of our model.

## 1.5 Conclusions

The excellent physical fidelity of the finite element magnetic diffusion model (1.30a)–(1.30c) stems from the fidelity of the finite element sequence  $\mathcal{W}^i$  to the fundamental

<sup>7</sup>This can be accomplished by setting  $\mathbf{B}_h^0 = \nabla \times \mathbf{A}_h^0$  for some potential  $\mathbf{A}_h^0 \in \mathcal{W}^1$ .

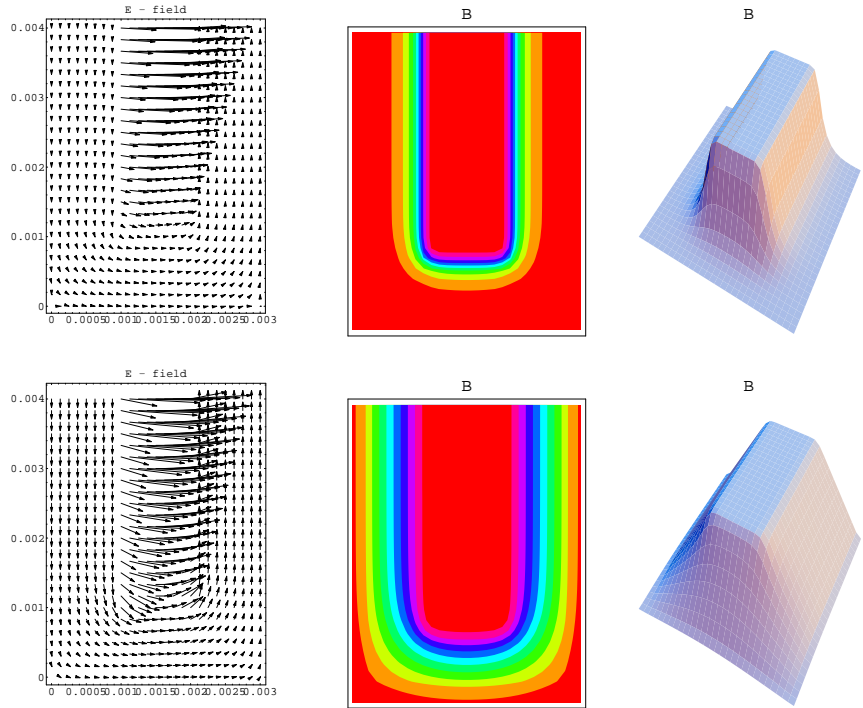
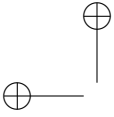


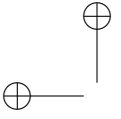
**Figure 1.8.** *Electric field and magnetic flux density at  $t_1$  and  $t_{steady}$ .*

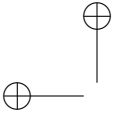
mathematical structure of the Maxwell's equations. Rather than being a mere functional approximation, the set  $\mathcal{W}^i$  represents a discrete model that captures the higher complexity of an exactness relation engendered by combination of spaces *and* operators.

In practical terms this translates into an ability to approximate well the kernels of fundamental differential operators, which in turn leads to a confinement of nonphysical modes to the zero frequency. The fact that exact sequences approximate well kernels also means that they necessarily lead to algebraic problems with large nullspaces. Special care must be taken in solving these problems, especially if fast and reliable algorithms are desired. Fortunately, in the past few years there has been a significant progress in extending multilevel solution techniques, including multigrid and algebraic multigrid, to algebraic systems obtained from exact sequences of finite element spaces; see e.g., [2], [20], and [28], among others. While it is true that these algorithms are, as a rule, more complex than standard nodal multilevel solvers, the exceptional fidelity of the discrete models makes the extra effort well worth the price. One should also keep in mind the additional benefits of exact sequences, such as simplicity of imposing tangential and normal boundary conditions and the possibility to customize the model so as to address different modeling goals.



In closing, let us mention that the notions of exactness and discrete De Rham complex are not limited to finite element settings. Similar concepts are found, either implicitly or explicitly, in the core of all successful discrete models of the Maxwell's equations, ranging from the original Yee scheme [33] and the finite integration technique (FIT) method of Weiland [31], to covolume schemes [26], and the recent mimetic schemes [22].

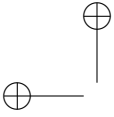




# Bibliography

- [1] ST. ADAM, P. ARBENZ, AND R. GEUS *Eigenvalue solvers for electromagnetic fields in cavities*. Technical Report 275, Institute of Scientific Computing, ETH Zürich, October 1997.
- [2] D. ARNOLD, R. FALK, AND R. WINTHER, *Multigrid in  $H(\Omega, \text{div})$  and  $H(\Omega, \text{curl})$* , Numer. Math., 85 (2000), pp. 197–217
- [3] O. BIRO AND K. PREIS, *On the use of the magnetic vector potential in the finite element analysis of three-dimensional eddy currents*, IEEE Trans. Magnetics, 25 (1989), pp. 3145–3159.
- [4] O. BIRO AND K. PREIS, *Finite element analysis of 3-D eddy currents*, IEEE Trans. Magnetics, 26 (1990), pp. 418–423.
- [5] P. BOCHEV, J. HU, A. ROBINSON AND R. TUMINARO, *Robust 3D Z-pinch simulations: discretization and fast solvers for magnetic diffusion in heterogeneous conductors.*, Technical Report SAND 2001-8363J, Sandia National Laboratories. To appear in ETNA.
- [6] P. BOCHEV AND A. ROBINSON *Formulations, gauges and boundary conditions for eddy current analysis in inhomogeneous conductors*, unpublished.
- [7] D. BOFFI, P. FERNANDES, L. GASTALDI, AND I. PERUGIA, *Computational models of electromagnetic resonators: analysis of edge element approximations*, SIAM J. Numer. Anal., 36 (1999), pp. 1264–1290
- [8] A. BOSSAVIT AND J. VERITE, *A mixed fem-biem method to solve 3-d eddy current problems*, IEEE Trans. Magnetics, 18 (1982), pp. 431–435.
- [9] A. BOSSAVIT, *A rationale for “edge-elements” in 3-D fields computations*, IEEE Trans. Magnetics, 24 (1988), pp. 74–79.
- [10] ———, *Computational Electromagnetism*, Academic Press, 1998.
- [11] ———, *On the Lorenz gauge*, COMPEL, 18 (1999), pp. 323–336.
- [12] D. BRAESS, *Finite elements. Theory, Fast Solvers, and Applications in Solid Mechanics*, Cambridge University Press, Cambridge, 1997.

- [13] F. BREZZI AND M. FORTIN, *Mixed and Hybrid Finite Element Methods*, Springer-Verlag, 1991.
- [14] C. F. BRYANT, C. R. I. EMSON, AND C. W. TROWBRIDGE, *A comparison of Lorenz gauge formulations in eddy current computations*, IEEE Trans. Magnetics, 26 (1990), pp. 430–433.
- [15] ———, *A general purpose 3-d formulation for eddy currents using the Lorenz gauge*, IEEE Trans. Magnetics, 26 (1990), pp. 2373–2375.
- [16] C. F. BRYANT, C. R. I. EMSON, C. W. TROWBRIDGE, AND P. FERNANDES, *Lorenz gauge formulations involving piecewise homogeneous conductors*, IEEE Trans. Magnetics, 34 (1998), pp. 2559–2562.
- [17] F. BREZZI, J. DOUGLAS AND D. MARINI, *Efficient rectangular mixed finite elements in two and three space variables*, M<sup>2</sup>AN Math. Model. Numer. Anal., 21 (1987), pp. 581–604.
- [18] S. CAORSI, P. FERNANDES, AND M. RAFFETTO, *On the spurious modes in deterministic problems*, COMPEL, Suppl. A, 13 (1994), pp. 317–332.
- [19] C. R. I. EMSON AND J. SIMKIN, *An optimal method for 3-D eddy currents*, IEEE Trans. Magnetics, 19 (1983), pp. 2450–2452.
- [20] R. HIPTMAIR, *Multigrid method for Maxwell's equations*, SIAM J. Numer. Anal., 36 (1998), pp. 204–225.
- [21] R. HIPTMAIR, *Canonical construction of finite element spaces*, Math. Comp., 68 (1999) pp. 1325–1346.
- [22] J. M. HYMAN, AND M. SHASHKOV, *Mimetic discretizations for Maxwell's equations*, J. Comput. Phys. 151 (1999), pp. 881–909.
- [23] F. KIKUCHI, *Mixed and penalty formulations for finite element analysis of an eigenvalue problem in electromagnetism*, Comp. Meth. Appl. Mech. Engrg., 64 (1987), pp. 509–521.
- [24] J. NEDELEC, *Mixed finite elements in  $\mathbf{R}^3$* , Numer. Math., 35 (1980), pp. 315–341.
- [25] ———, *A new family of finite element methods in  $\mathbf{R}^3$* , Numer. Math., 50 (1986), pp. 57–81.
- [26] R. NICOLAIDES, *Direct discretization of planar div-curl problems*, SIAM J. Numer. Anal. 29 (1992), pp. 32–56
- [27] B. RAHMAN AND J. DAVIES, *Penalty function improvement of waveguide solution by finite elements*, IEEE Trans. Microwave Theory and Techniques, 32 (1984), pp. 922–928.



- 
- [28] S. REITZINGER AND J. SCHÖBERL, *Algebraic multigrid for finite element discretizations with edge elements*. Unpublished manuscript. [reitz@sfb013.uni-linz.ac.at](mailto:reitz@sfb013.uni-linz.ac.at).
- [29] G. TOTH, *The  $\nabla \cdot B = 0$  constraint in shock-capturing magnetohydrodynamic codes*, J. Comput. Phys., 161, (2000) pp. 605–652.
- [30] J.S. WANG AND N. IDA, *Curvilinear and higher order edge finite elements in electromagnetic field computation*, IEEE Trans. Magnetics, 29 (1993), pp. 1491–1494.
- [31] T. WEILAND, *Numerical solution of Maxwell's equations for static, resonant and transient problems*, in *Studies in Electrical and Electronic Engineering 28B*, T. Berceci, ed., URSI International Symposium on Electromagnetic Theory Part B, Elsevier, New York (1986), pp. 537–542.
- [32] J. S. VAN WELIJ, *Calculation of eddy currents in terms of  $H$  on hexahedra*, IEEE Trans. Magnetics, 21 (1985), pp. 2239–2241.
- [33] K. S. YEE, *Numerical solution of initial boundary value problems involving Maxwell's equations in isotropic media*, IEEE Trans. Antennas and Propagation, 14 (1966), pp. 302–307
- [34] G. YONAS, *Fusion and the Z-pinch*, Scientific American, 279/2, (1998) pp. 22–27.